Article

Not peer-reviewed version

# Enhancing Starch-Based Packaging Materials: Optimization of Plasticizers and Process Parameters

Yue Wu [†], Rongji Tang [†], Anfu Guo [*], Xiaodong Tao, Yingbin Hu, Xianliang Sheng, Peng Qu, Shaoqing Wang, Jianfeng Li, Fangyi Li

Posted Date: 1 August 2023

doi: 10.20944/preprints202308.0045.v1

Keywords: Plasticizer plasticizing; Thermoplastic starch; Box–Behnken design; Response surface method; Starch-based composite packaging material

*Article*

# Enhancing Starch-Based Packaging Materials: Optimization of Plasticizers and Process Parameters

**Yue Wu [1,†], Rongji Tang [1,†], Anfu Guo [1,*], Xiaodong Tao [1], Yingbin Hu [2], Xianliang Sheng [1], Peng Qu [1], Shaoqing Wang [1], Jianfeng Li [3] and Fangyi Li [3]**

[1] School of Mechanical and Automotive Engineering, Liaocheng University, Liaocheng, Shandong 252000, China
[2] Department of Mechanical and Manufacturing Engineering, Miami University, Oxford, OH, 45056, USA
[3] School of Mechanical Engineering, Shandong University, Jinan, Shandong 250061, China
* Correspondence: guoanfu@lcu.edu.cn.
† These authors contributed to the work equally and should be regarded as co-first authors.

**Abstract:** Due to the non-degradability of petroleum-based packaging materials, serious environmental pollution and the depletion of non-renewable resources have become pressing issues. In order to actively promote green production and address these concerns, there is an urgent need for new packaging materials to replace traditional plastic products. Starch-based packaging materials, composed of starch, fiber, and plasticizers, offer a degradable and environmentally friendly alternative. Starch alone cannot undergo thermoplastic processing due to its inherent structural characteristics. Therefore, researchers have explored modifications by incorporating plasticizers to create processable thermoplastic starch (TPS). However, there are challenges related to the high crystallinity and poor compatibility between TPS and fibers, resulting in decreased mechanical properties. To address these challenges, a novel approach combining plasticizer optimization and response surface method (RSM) optimization has been proposed to enhance the mechanical properties of starch-based packaging materials. This method leverages the advantages of composite plasticizers and process parameters. The findings demonstrate that the composite plasticizer effectively disrupt the hydrogen bonding and granule morphology of starch, leading to a significant reduction in crystallinity. Based on these findings, the optimal process parameters are determined using the RSM, resulting in a forming temperature of 198 °C, forming time of 5.4 minutes, and AC content of 0.84 grams. Compared with the non-optimized values, the tensile strength increases by 12.2% and the rebound rate increases by 8.1%.

**Keywords:** plasticizer plasticizing; thermoplastic starch; Box–Behnken design; response surface method; starch-based composite packaging material

## 1. Introduction

Packaging materials derived from petroleum-based plastics are non-biodegradable, leading to severe pollution of the environment upon which humans depend [1–3] and posing a significant threat to human health [4–6]. As a result, numerous researchers have turned their attention to biomass materials, which are obtained from natural sources and can undergo complete degradation. Examples of such biomass materials include corn, wheat, sorghum, and others [7–9]. By combining these materials with fibers and incorporating a foaming agent, it is possible to prepare a biomass packaging material with a cellular structure [10].

Among various biomass materials, starch has gained recognition as an environmentally friendly material due to its easy availability, economic benefits, and ability to completely decompose into carbon dioxide and water under natural conditions [11,12]. Starch molecular chains contain a significant number of hydroxyl (–OH) groups, which readily undergo hydrogen bonding with each other, promoting the formation of a dispersed microcrystalline structure known as the double helix structure [13]. During the gelatinization process of starch, water molecules disrupt the hydrogen bonding mechanism of starch, causing the double helix structure to unwind and stretching the starch molecular chains [14]. However, at this stage, the starch molecular chains are not stable, and over

 doi:10.20944/preprints202308.0045.v1



time, the hydrogen bonding tends to reform, leading to the formation of different ordered structures, known as retrogradation [15]. The presence of glucoside bonds (C-O-C) and –OH groups on the starch molecular chains results in strong intermolecular forces, low molecular chain mobility, and limited relative sliding. This unique structure gives starch a decomposition temperature lower than its melting temperature, making it unsuitable for direct thermoplastic processing [16,17]. Therefore, the structure of starch needs to be modified or disrupted.

Currently, the most common method of disrupting the hydrogen bonding mechanism and modifying the structure of starch is through the use of plasticizers, which enhance the thermoplastic processing performance and ensure the compatibility of starch with other polymers [18–20]. Avila-Martin et al. [19] extracted starch film from canna roots and introduced citric acid and whey protein isolate as modifiers. The results demonstrated that both citric acid and whey protein isolate effectively plasticized the starch film, leading to more uniform hydrogen bonding and improved material durability. Zeng et al. [20] investigated the modification of NCS using glycerol (GLY) and urea as composite plasticizers. The study revealed that the addition of 15 parts per hundred resulted in plasticized NCS and a composite with favorable mechanical properties. Among various plasticizers, GLY, as a safe and harmless small molecule polyol, exhibits high mobility and can disrupt the original hydrogen bonding mechanism of starch, reducing its crystallinity and glass transition temperature, thus conferring thermoplastic processing properties [21,22]. However, the hydrogen bond between GLY and starch is relatively weak, making it prone to retrogradation after long-term storage [23]. D-fructose, as a monosaccharide plasticizer with a larger molecular weight, can form better bonds with hydrogen in starch [24]. Furthermore, Saberi et al. [25] suggested that sugar plasticizer molecules interact with water molecules during the plasticization process, inhibiting the recrystallization process and preventing retrogradation. Therefore, in this investigation, GLY and D-fructose are selected as plasticizers to investigate the effects of individual and combined effects on starch.

The investigation of plasticizers has facilitated the development of TPS. However, in the actual preparation and production of starch-based packaging materials, it is necessary to incorporate natural fibers into the starch matrix. Nevertheless, the high crystallinity and poor biocompatibility between the two components significantly impact their mechanical properties [26–28]. Various methods such as oxidation [29], esterification [30], and graft copolymerization [31,32] are commonly employed to enhance these properties. Zhang et al. [29] prepared oxidized starch using an oxidant and successfully utilized GLY as a plasticizer to create thermoplastic oxidized starch with favorable rheology and toughness. The study revealed the formation of new hydrogen bonds between the plasticizer, oxidant, and starch, resulting in a combination of oxidation and plasticization effects. This led to changes in the crystal structure of oxidized starch and significantly improved its pressure resistance. Chen et al. [30] produced a starch composite through oxidative esterification. In comparison to natural starch composites, the starch composite produced through oxidative esterification exhibited higher structural damage, lower crystallinity, and notable improvements in toughness and tensile strength. Zha et al. [32] grafted hydrophilic polyacrylic acid branches onto a starch acetate framework using water as the medium. The study demonstrated that the hydrophilic polyacrylic acid branches effectively reduced the crystallinity of starch acetate, mitigated film brittleness, and enhanced the adhesion of starch acetate to fibers and films.

In addition to the aforementioned methods, the mechanical properties of the composite materials can also be significantly influenced by the process parameters in the forming process. Perez-Chavez et al. [33] utilized an extrusion process to produce a flame-retardant polymer composite. By optimizing the keratin fiber length, blending temperature, and rotation speed during the forming process using the RSM, they achieved a balance between flame retardancy and mechanical properties, resulting in a flame-retardant bio-composite with a tensile strength of 0.6 ± 39.4 MPa. However, few researchers have investigated the combination of plasticizer optimization and optimization of process parameters in thermal cavity forming.

In this study, GLY, D-fructose, and their mixture have been employed as plasticizers to modify starch to make it processable for the first time. The optimal mass ratio between the natural corn starch

Preprints (www.preprints.org) | NOT PEER-REVIEWED | Posted: 1 August 2023 doi:10.20944/preprints202308.0045.v1



(NCS), the GLY, and the D- fructose has been determined. Subsequently, the prepared TPS is blended with pre-fabricated sisal fibers and processed in a thermal cavity forming machine after adding a foaming agent, resulting in a starch-based packaging material with a bubble structure. During the forming process in the thermal cavity, the RSM is utilized to investigate the effects of forming temperature, forming time, and foaming agent content on the tensile strength and rebound rate. Then, the optimal process parameters are determined.

## 2. Materials and Experimental Procedures

### *2.1. Materials preparation and experimental set-up*

In this study, NCS (Huachen Starch Sugar Co., LTD., Hebei, China) was used as the substrate. Sisal fibers (Li Qiang Fiber Industry Co., LTD., Chongzuo, Guangxi, China) with an average length of 5 mm and an average diameter of 60 μm were used as reinforcement material. GLY ($C_3H_8O_3$, Fuyu Fine Chemical Co., LTD., Tianjin, China) and D-fructose (Chengchuan Technology Co., LTD., Shandong, China) were used as the plastic agents. The molecular structures of GLY and D-fructose are shown in Figure 1.

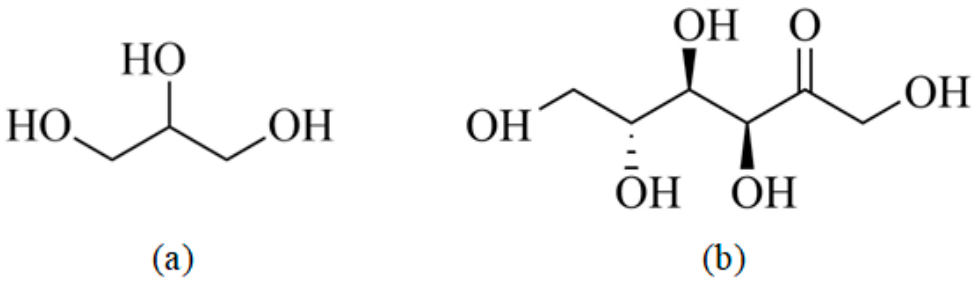


**Figure 1.** Molecular structures of plasticizers: (a) GLY, and (b) D-fructose.

AR-grade azodiacarbonamide (AC, Ruian in rubber and plastic additives Co., Ltd., Zhejiang, China) was used as the blowing agent. AR-grade tricarboxylic acid was used as the release agent (Guangcheng Chemical Co., LTD., Tianjin, China).

The preparation process of the starch-based packing structure is provided in Figure 2.

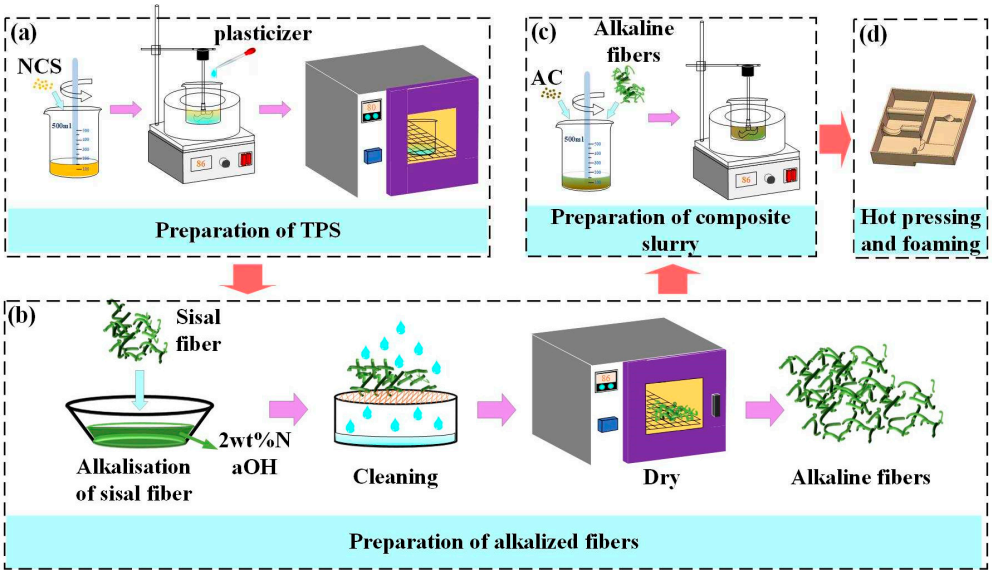


**Figure 2.** The preparation process of the starch-based packaging materials: (a) preparation of the TPS, (b) alkalization treatment of the sisal fibers, (c) preparation of the composite slurry, and (d) hot pressing and foaming.

Preprints (www.preprints.org) | NOT PEER-REVIEWED | Posted: 1 August 2023 doi:10.20944/preprints202308.0045.v1



Firstly, the NCS and distilled water (Shuangshuang Chemical Co., LTD., Yantai, Shandong, China) were mixed with a mass ratio of 1: 3 in a beaker. Then, a glass rod was used to stir the mixture slowly until the starch is completely dissolved. Then, the mixture was kept at 86 °C in a water bath (Joanlab, Huzhou, Zhejiang, China), and was stirred for 30 minutes using a precision force mixer (JJ-1, Shibo Experimental Instrument Factory, Changzhou, Jiangsu, China). Afterward, the plasticizer (GLY, D-fructose) was added to the beaker at different mass ratios according to Table 1. The new mixture was stirred at high speed until the starch was completely gelatinized. Then, the new mixture was kept at 86 °C in a water bath for 12 hours.

**Table 1.** Mass ratio of NCS to different plasticizers.

| NCS: GLY | NCS: D-fructose | NCS: GLY: D-fructose |
|---|---|---|
| 10: 1 | 10: 1 | 10: 1: 1 |
| 10: 2 | 10: 2 | 10: 2: 1 |
| 10: 3 | 10: 3 | |
| 10: 4 | 10: 4 | |

The resulting gelatinized starch was dried in a vacuum drying oven at 80 °C for 24 hours to obtain TPS, as shown in Figure 2(a). Then, the sisal fiber was soaked in a 2 wt.% NaOH solution for 8 hours, removed, washed repeatedly with distilled water until the pH value reached 7, and dried in a drying box at 86 °C for 12 hours to obtain the alkalized fiber, as shown in Figure 2(b). Finally, the TPS, alkalized fiber, and blowing agent were thoroughly mixed in a high-speed mixer with a mass ratio of 10: 3: 0.1 to obtain a composite slurry, as shown in Figure 2(c). The composite paste was placed in the lower mold of a self-made double-column simplex thermal cavity forming machine (Figure 3(a)), and the mold temperature was set at 198 °C. Subsequently, the upper mold was moved down, the mold was closed, and the slurry was deformed, as depicted in Figure 3(b). The resulting starch-based packaging material is shown in Figure 2(d).

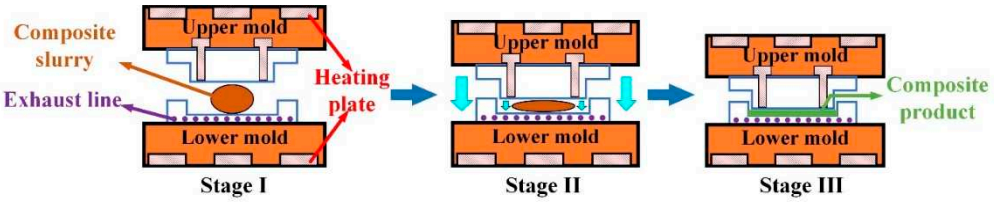


**Figure 3.** The experimental process of the thermal cavity forming experimental device.

The foaming process is depicted in Figure 4. In the transition from the first stage to the second stage, as the temperature increases, the viscosity of TPS gradually rises. This leads to the evaporation of water, decomposition of AC, and release of water vapor, nitrogen, and carbon monoxide, which provide gases for pore growth. Moving from the second stage to the third stage, TPS is gradually compressed and tightly encases the sisal fiber during the curing process. Ultimately, a cellular structure is formed, where the sisal fiber acts as the skeleton and starch serves as the matrix.

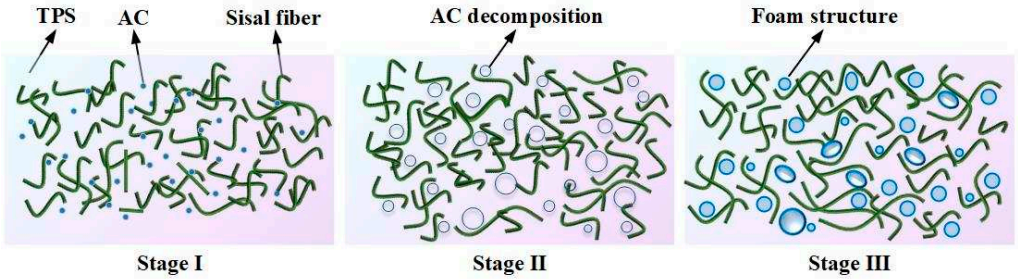


**Figure 4.** A diagram showing the three major stages of the foaming process.

 doi:10.20944/preprints202308.0045.v1



*2.2. Material characterizations*

A portion of the TPS prepared in 2.1 was subjected to drying in a drying box at 60 °C for 24 hours to remove moisture. After thorough grinding, it was strained through a 200-mesh screen and left at room temperature for 30 days. A sample of 1 mg of TPS was taken and mixed with 150 mg of potassium bromide, then pressed into a transparent sheet. Fourier Transform Infrared Spectroscopy (FT-IR) (NICOLET-IR200, Thermo Fisher Scientific Company, Shanghai, China) was employed to detect and analyze the effect of plasticizers on the hydrogen bonds of starch within the spectral range of 500-4000 $cm^{-1}$. Scanning was recorded with a resolution of 2 $cm^{-1}$. X-ray Diffraction (XRD) (SmartLab 9 kW, Japan) was utilized to analyze the changes in crystal types before and after starch modification. The scanning speed was set at 5°/min, and the analysis angle ranged from 10° to 80°. Scanning Electron Microscopy (SEM) (Phenom XL-SE, Netherlands) was employed to examine the impact of plasticizers on the micromorphology of starch.

*2.3. Mechanics Performance Testing*

Tensile specimens were prepared following the guidelines outlined in GB/T9641-88. The tensile test was conducted using the Electronic Universal Material Experimental machine (KX WDW3200, Kexin Experimental Instrument Co., LTD, Changchun, Jilin, China) at a constant speed of 5 mm/min. To minimize experimental errors, five trials were performed for each composite material. The compressed sample was prepared in accordance with the GB/T 8186-2008 standard, with a sample size of 25 mm (Length) × 25 mm (Width) × 5 mm (Height). The compression test machine was set to a speed of 12 mm/min. The original thickness of the sample was maintained, and the load was gradually applied in the direction perpendicular to the thickness. Once the sample underwent 30% deformation, the stable load was maintained for the duration of 3 minutes. Afterward, the sample was unloaded and left for 30 seconds. The thickness of the compressed specimen was measured using a spiral micrometer, and the rebound rate was calculated. Each group of experiments was repeated three times, with an interval of 1 minute between each experiment. The average result from the three repetitions was considered as the rebound rate for that particular sample group. The formula for calculating the rebound rate is:

$$t_j = \frac{T_j - {T_j}/{2}}{{T_i}/{2}} \times 100\% \quad (1)$$

Where, $t_j$ is the rebound rate after j experiments; $T_j$ is the thickness of the specimen after j times compression, mm; $T_i$ is the original thickness of the sample, mm. i and j are the number of experiments.

*2.4. Process parameter optimization*

A starch-based biomass packaging material with a bubble cell structure was prepared using TPS as the matrix, alkalized sisal fiber as the reinforcement, and azodicarbonamide (AC) as the blowing agent. The thermal cavity forming process was employed for fabrication. The RSM was utilized to optimize the process parameters, with the variables being forming temperature, forming time, and AC content. The response values considered for optimization were rebound rate and tensile strength. A regression model was fitted, and variance analysis was conducted to optimize the forming process. Each factor was designed with three levels, as presented in Table 2. The experiment was performed 17 times, with the central point repeated 5 times.

**Table 2.** Different levels of process parameters.

| level | Forming temperature (°C) | Forming time (min) | AC content (g) |
|---|---|---|---|
| -1 | 195 °C | 4 | 0.5 |
| 0 | 205 °C | 5 | 1 |
| 1 | 215 °C | 6 | 1.5 |

Preprints (www.preprints.org) | NOT PEER-REVIEWED | Posted: 1 August 2023 doi:10.20944/preprints202308.0045.v1



The three input variables were optimized based on the following steps.

1. Establishing a general mathematical relationship between the input variables and response, which can be expressed as:

$$Y=f\ (X_1, X_2, X_3 \ldots \ldots, X_n) \quad (2)$$

where $Y$ is the response, $f$ represents the mathematical relationship, and $X_1$, $X_2$, $X_3$… …, $Xn$ are input variables.

2. Looking for mathematical models. Based on mathematical analysis, the existing McLaughlin or Taylor expansions can meet convergence conditions. According to Samir Charola et al. [34], the experimental data can be fitted into a second-order polynomial model, namely,

$$Y=\beta_0+\sum_{i=1}^{k}\beta_i x_i+\sum_{i=1}^{k}\beta_{ii} x_i^2+\sum_{i>j}^{k}\sum_{j}^{k}\beta_{ij} x_i x_j \quad (3)$$

where $\beta_0$, $\beta_i$, $\beta_{ij}$, and $\beta_{ii}$ are the regression coefficients of the intercept, the linearity, the interaction, and the quadratic terms, respectively. $x_i$ and $x_j$ denote the input variables, and k represents the number of input variables selected for process optimization.

3. Using analysis of variance (ANOVA) to evaluate the significance of the prediction model. The reliability of the model can be determined by loss of fit (LOF) and P value. The actual values are the tensile strength and rebound rate measured by experiments. Based on the second-order polynomial model, the response surface and the contour plot which describe the influences of two variables on a single target can be obtained. The third input variable remains unchanged at the center point. Then, the effects of input variables on the response will be analyzed to obtain the highest rebound rate and the tensile strength simultaneously.

## 3. Results and Discussion

### *3.1. The plasticization process of starch*

Starch is considered as a natural polycrystalline system. Crystalline, submicron crystalline, and amorphous structures alternate to form the granular structure of starch. Under the combined action of plasticizers, temperature, and moisture, the inherent crystalline structure of starch is disrupted, resulting in a lower glass transition temperature and obtaining thermoplastic processing properties. The plasticization process of starch can be divided into four stages, as shown in Figure 5.

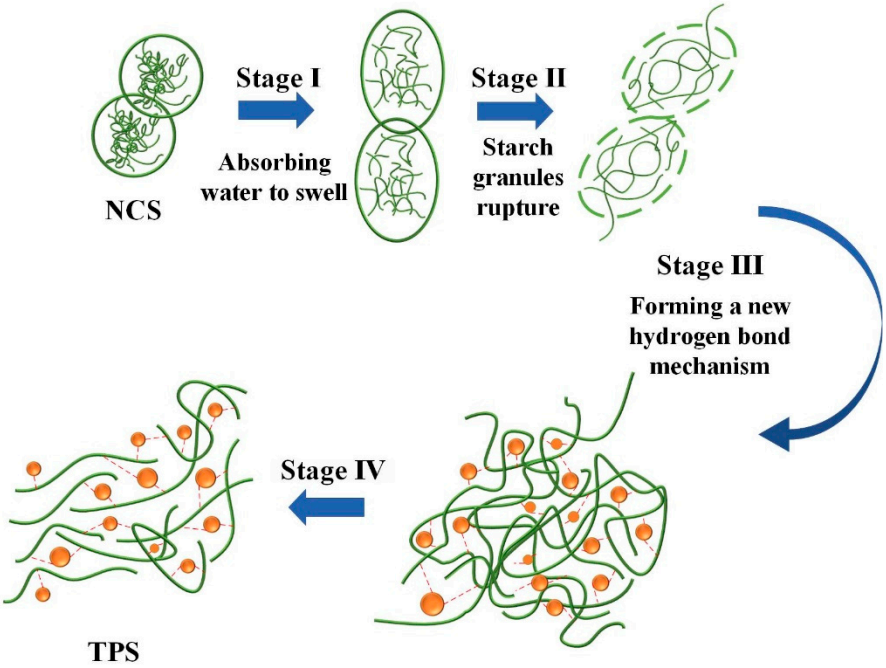


**Figure 5.** The four stages of the starch plasticization process.

Preprints (www.preprints.org) | NOT PEER-REVIEWED | Posted: 1 August 2023 doi:10.20944/preprints202308.0045.v1



Stage I: Starch absorbs water and swells. Natural starch aggregates in the form of granules. When subjected to distilled water, the starch granules absorb water and swell, which is also known as reversible water absorption and swelling. During this process, water absorption occurs in the amorphous regions of the starch, while the crystalline regions remain intact. Once the water disperses, the starch can revert back to its original granular structure.
Stage II: Starch granules break. As the ambient temperature increases, under the combined action of plasticizers, mechanical agitation, and moisture, the starch granules begin to break.
Stage III: New hydrogen bonding mechanism forms. Under the action of thermal and continuous mechanical agitation, plasticizer molecules enter the interior of starch granules, disrupting the existing hydrogen bonds. The entire molecules undergo relaxation, resulting in a destruction of the crystalline structure and an increase in the number of free branching chains, thereby increasing the free volume within the starch. At the same time, the plasticizer molecules provide a large number of –OH groups, making them more prone to interact with the –OH groups in starch. The resulting starch-plasticizer hydrogen bonding mechanism replaces the original starch-starch hydrogen bonding mechanism.
Stage IV: Plasticized starch forms. Under the influence of the new hydrogen bonding mechanism, starch molecules undergo rearrangement, leading to increased molecular chain mobility and a decrease in melting temperature. As a result, starch acquires processability.

In the plasticization process, plasticizers play a crucial role by primarily disrupting the hydrogen bonding in starch. The mechanism of their action is illustrated in Figure 6. Plasticizers enter the interior of starch and interact with the –OH groups on starch molecules, forming new hydrogen bonding mechanisms.

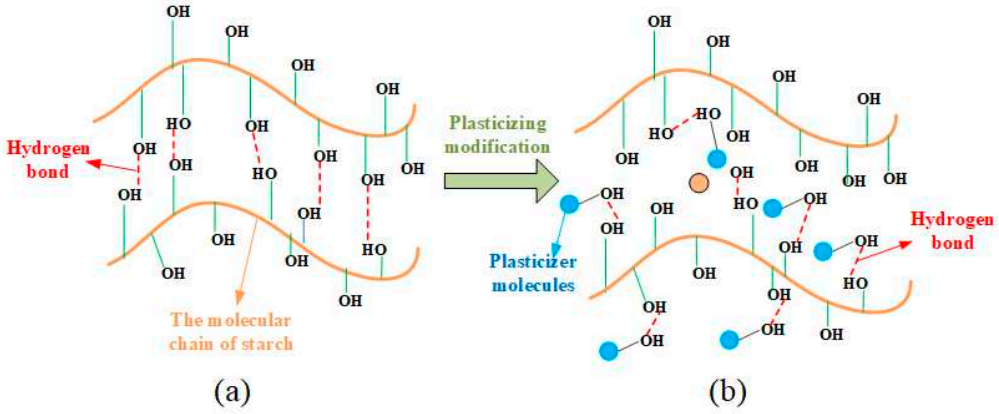


**Figure 6.** Plasticizer's effects on disrupting the hydrogen bonding in starch: (a) Before adding the plasticizer and (b) after adding the plasticizer.

### *3.2. Effects of plasticizer on TPS*

#### 3.2.1. Effects of plasticizer on hydrogen bond

Figure 7(a) shows the infrared spectral images of the NCS, and the starch with different proportions of GLY plasticizer additions. In infrared spectrum detection, when the hydrogen bond is strengthened, the vibration frequency of –OH group will decrease, and the vibration spectrum band will become wider. This can be attributed to the fact that the strength of the hydrogen bond can affect the vibration mode of the –OH group, thus making it more difficult to be excited. The strength of the hydrogen bond is determined by the combined influence of the hydrogen bond length, angle, as well as the electric charge density at the center of hydrogen bond. In addition, the establishment of hydrogen bond elongates the bond length of –OH group, increase the vibration absorption energy, and drive the absorbance shift to the low frequency. It is known that the frequency equals the energy of the wave multiplies the speed of light. The more the number of waves moves, the stronger the hydrogen bond will be [35].

Preprints (www.preprints.org) | NOT PEER-REVIEWED | Posted: 1 August 2023 doi:10.20944/preprints202308.0045.v1



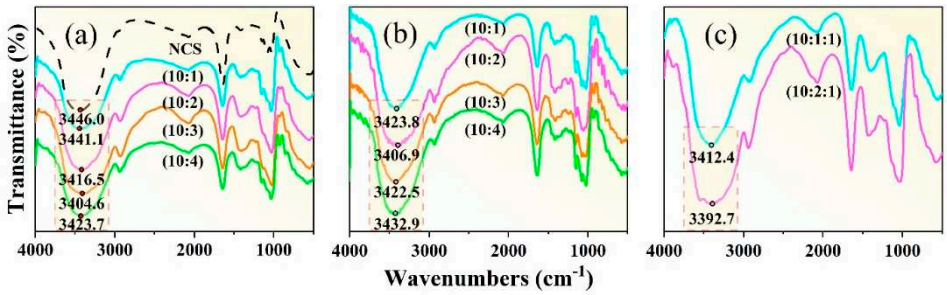


**Figure 7.** Infrared spectra: (a) GLY is the plasticizer, (b) D-fructose is the plasticizer, and (c) GLY and D-fructose is the composite plasticizer.

The infrared spectrum of NCS (black dashed line in Figure 7(a)) shows that the absorption peak of the -OH occurs at 3446 $cm^{-1}$. With the increase of GLY content, the frequency of the absorption peak gradually decreases to 3441.1 $cm^{-1}$, 3416.5 $cm^{-1}$, 3404.6 $cm^{-1}$, and 3423.7 $cm^{-1}$, indicating that a new hydrogen bond is formed between GLY and starch molecules. When the mass ratio between starch and GLY is 10: 3, the vibration frequency of –OH group is the lowest, and the spectrum is wide, indicating that the hydrogen bond is the strongest and the plasticization effect is the best at this mass ratio. When the GLY content increases until the mass ratio between starch and GLY reaches 10: 4, the absorption peak of the –OH wave tends to shift to higher frequency, indicating that an excessive GLY addition was not conducive to the plasticization process of starch. This might be attributed to the fact that the excess GLY itself also forms hydrogen bonds, of which one –OH and the other –OH forms a hydrogen bond, thus enhancing the stability of the GLY and reducing the plasticization effect.

In the plasticization process, there are a large number of –OH groups in starch molecules. In the process of forming covalent molecules between the hydrogen atoms in the –OH groups and the electronegative oxygen atoms, the electrons from the hydrogen atoms are shared on chemical bonds, and are strongly attracted by neighboring atoms. Therefore, the electron clouds of the hydrogen atoms are away from the hydrogen nuclei and the shared electron pairs between atoms, and the hydrogen atoms show positive $H^+$. GLY contains a significant number of electronegative oxygen atoms. In the process of penetrating starch granules, small molecular weight GLY and $H^+$ react to generate a magnetic field, which destroys the hydrogen bonds within starch. Due to the action of van der Waals force [36], the GLY and $H^+$ are directionally aligned with a formation of a new hydrogen bond structure.

Figure 7(b) shows the effects of D-fructose plasticizer contents on infrared spectra of TPS. Results show that when the mass ratios between starch and D-fructose plasticizer are 10: 1, 10: 2, 10: 3, and 10: 4, the absorption peak frequencies are located at 3423.8 $cm^{-1}$, 3406.9 $cm^{-1}$, 3422.5 $cm^{-1}$, and 3432.9 $cm^{-1}$, respectively. Therefore, it can be concluded that hydrogen bonds are formed between starch molecules and D-fructose molecules, and the D-fructose has a plastic effect on the starch. Particularly, the absorption peak frequency is the smallest when the mass ratio of starch to fructose is 10: 2. At this mass ratio, the number of hydrogen bonds is the largest and the hydrogen bonds are the most stable. When the fructose content continues to increase, hydrogen bonds tend to form between fructose molecules. Excessive accumulation of fructose in the starch matrix affects its plasticization effect. The D-fructose has a high molecular weight, and the number of –OH that can form hydrogen bonds with the starch is large. Therefore, D-fructose is less likely to precipitate after plasticization and can improve the stability of the starch matrix [24].

It is worth noting that both GLY and D-fructose have certain shortcoming when using each of them alone. GLY has a small molecular weight and it can effectively penetrate starch granules. However, the GLY is also prone to precipitate, and the retrogradation problem of GLY-plasticized starch plasticized cannot be ignored [23]. The molecules of D-fructose can stabilize the starch matrix by restricting the fluidity and flexibility of starch chains and inhibiting recrystallization and retrogradation phenomena [25], but its molecular weight is too large to enter adjacent starch molecule chains. Therefore, combining both of them to produce a composite plasticizer is necessary.

 doi:10.20944/preprints202308.0045.v1



To explore the synergistic plasticization ability of the composite plasticizer on NCS, NCS with different composite plasticizers are prepared, as shown in Figure 7(c). When the mass ratio between NCS, GLY, and D-fructose changes from 10: 1: 1 to 10: 2: 1, the –OH stretching vibration peaks within the wavenumbers of 3645 $cm^{-1}$~3300 $cm^{-1}$ exhibit a trend of decreasing frequency, indicating that the plasticization effect of the composite plasticizer is better than that of single plasticizers. When the mass ratio between NCS, GLY, and D-fructose is 10: 2: 1, the vibration frequency of O–H is 3392.7 $cm^{-1}$, and the absorption peaks show a clear trend of broadening. Therefore, the synergistic plasticization effect at this mass ratio is the best, and the greatest impact is achieved for the hydrogen bond structure of starch.

3.2.2. Effects of plasticizer on crystallization type

Figure 8(a) displays XRD images of TPS obtained using different proportions of NCS and GLY as plasticizers.

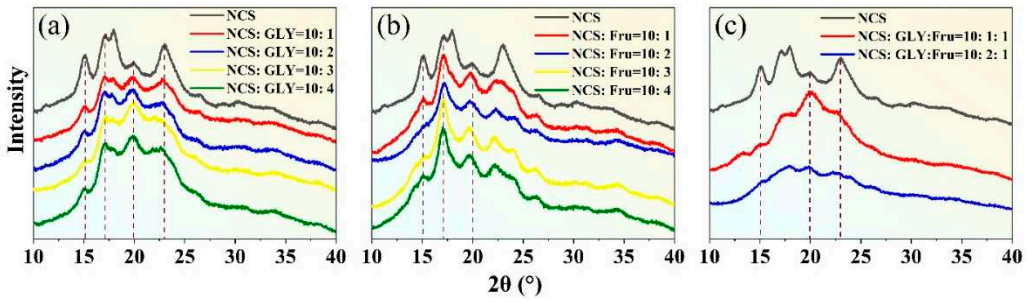


**Figure 8.** Effects of plasticizer content on XRD results when (a) GLY is the plasticizer, (b) D-fructose (Fru) is the plasticizer, and (c) GLY and Fru is the composite plasticizer.

NCS exhibits a combination of sharp crystal diffraction peaks and amorphous diffuse wide peaks, with its crystallinity primarily derived from amylopectin. The crystalline structures of NCS can be classified into A, B, and C types based on XRD analysis. Among them, the A-type crystal is highly ordered, and it belongs to the monoclinic crystal system, while the B-type crystal exhibits secondary order and it belongs to the orthorhombic system. C-type crystal represents a mixture of type A and type B, characterized by an unstable crystal structure [37]. NCS contains 72% amylopectin, which forms a stable double helix structure through hydrogen bonding and it belongs to A-type crystal. The main crystalline peaks are observed around 2θ = 15°, 17°, 18°, and 23°. When GLY is added as a plasticizer, it disrupts the original crystalline structure within the NCS, affecting the crystalline region. The original crystalline peaks (15°, 17°, 18°, 23°) become weaker, and the dispersed broad peaks become dominant. The dispersed broad peaks represent the residual natural crystalline after the plasticization process of the NCS, and it indicates that the preparation of TPS is insufficient to completely disintegrate the starch granules [38]. Notably, the diffraction peak near 2θ = 19.8° represents a typical $V_H$-type crystalline structure induced during the plasticization process [39]. This is attributed to the lubrication effect of small GLY molecules that penetrate and disrupt the starch granules. Under specific temperature and external force conditions, GLY infiltrates the interior of the starch, breaking the original hydrogen bonding and reducing the crystalline region. Over time, the branched starch molecules recombine to form a $V_H$-type crystalline structure.

Figure 8(b) presents XRD images of TPS obtained using D-fructose at different proportions as a plasticizer. The images indicate that the crystalline structure of NCS modified by D-fructose is partially disrupted. The XRD pattern displayed sharp characteristic peaks near 17°, which can be attributed to the rearrangement of the double helix structure after NCS molecule dehydration. As the content of D-fructose increases, the intensity of the crystallization peak gradually weakens. When the starch-to-fructose mass ratio reaches 10: 2, the diffraction peak becomes the weakest, and the peak at 15° completely disappears, indicating the strongest detrimental effect on the starch's crystalline structure. This suggests that within a certain range of D-fructose content, it can form new hydrogen bonds with starch molecules, weaken the inherent hydrogen bonding of starch, disrupt the

 doi:10.20944/preprints202308.0045.v1



crystallization zone, and increase the number of free branched chains. Additionally, a new $V_H$-type crystal peak appears near 20°, further confirming the disruption of the original starch crystal structure. It is important to note that D-fructose possesses more hydroxyl groups, larger spatial gaps with starch molecules, and increased cross-linking, enabling the formation of more stable hydrogen bonds with starch molecules. Furthermore, the C=O double bonds (Figure 1(b)) exhibit stronger electronegativity, resulting in denser electron clouds around oxygen atoms and facilitating the formation of new hydrogen bonds with starch molecules.

To enhance the plasticization effect, a combination of plasticizers, namely GLY and D-fructose, is used as they individually have limited ability to break down starch granules. Figure 8(c) displays the XRD pattern of plasticized starch prepared using a composite plasticizer. When the mass ratio between NCS, GLY, and D-fructose is 10:2:1, no significant diffraction peak is observed. This indicates that the plasticization effect is optimal at this mass ratio, as it effectively disrupts the crystalline structure of starch and inhibits starch retrogradation.

3.2.3. Effects of plasticizer on micromorphology

During the plasticization process of NCS, the crystal structure undergoes destruction, resulting in changes to the starch granules and their microscopic morphology. To further characterize the impact of plasticization modification on starch granules, it is necessary to analyze the changes in their microstructure. Figure 9 presents SEM images of three types of plasticized starch.

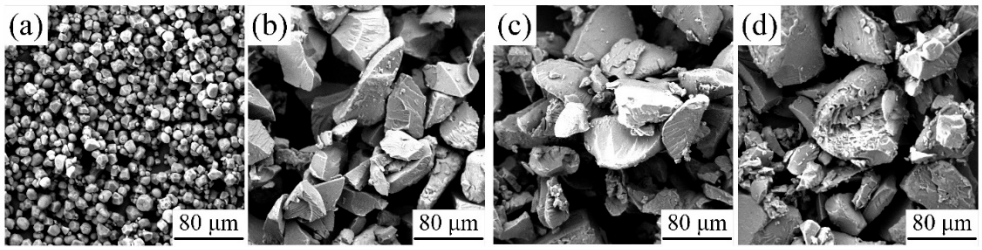


**Figure 9.** SEM images of the (a) NCS, the (b) NCS with GLY as the plasticizer, the (c) NCS with D-fructose as the plasticizer, and the (d) NCS with the GLY and D-fructose as the composite plasticizer.

Figure 9(a) illustrates the microstructure of NCS, which exhibits regular hexagonal-shaped granules with a smooth surface. The distribution of angularity is not prominent, and the overall shape is nearly spherical. Figure 9(b) displays the microstructure of GLY-plasticized starch, where the starch granules appear angular, elongated, and diamond-shaped, with a rough surface. Figure 9(c) showcases the microstructure of D-fructose-plasticized starch, revealing the clumping of starch granules and a small amount of granule detachment. Figure 9(d) presents the microstructure of GLY and D-fructose composite-plasticized starch, which demonstrates significant damage to the starch granules, characterized by evident holes, a rough surface, and raised small granules. In summary, the microstructure of NCS experiences noticeable damage when subjected to different plasticizers, with the most significant damage observed when composite plasticizers are employed.

*3.3. Molecular linking model of starch-based composites*

To analyze the cross-linking between NCS, plasticizer, and plant fiber, a molecular linkage model is developed and depicted in Figure 10. Sisal fiber is subjected to alkalization treatment to dissolve hemicellulose and pectin present in the fiber. During the alkalization process, sisal fiber reacts with NaOH, resulting in the formation of alkaline cellulose, as shown in Equation (4) [40]. Alkaline cellulose further ionizes to generate negatively charged alkaline cellulose anions, as depicted in Equation (5) [41]. When the –OH group on the plasticizer is in proximity to the O- group on the carboxymethyl of the fiber molecule, their strong magnetic fields attract each other, forming a new hydrogen bond. Furthermore, the free –OH group on the cellulose molecule also forms hydrogen bonds with the –OH group on the plasticizer. In summary, a stable structure of starch-plasticizer-

Preprints (www.preprints.org) | NOT PEER-REVIEWED | Posted: 1 August 2023 doi:10.20944/preprints202308.0045.v1



fiber, with the plasticizers (GLY, D-fructose) serving as bridges, is formed during the preparation of the mixed slurry.

$$[C_6H_7O_2(OH)_3]n+nNaOH \rightarrow [C_6H_7O_2(OH)_2ONa]n+nH_2O \quad (4)$$

$$[C_6H_7O_2(OH)_2ONa]n \rightarrow [C_6H_7O_2(OH)_2O^-]n+nNa^+ \quad (5)$$

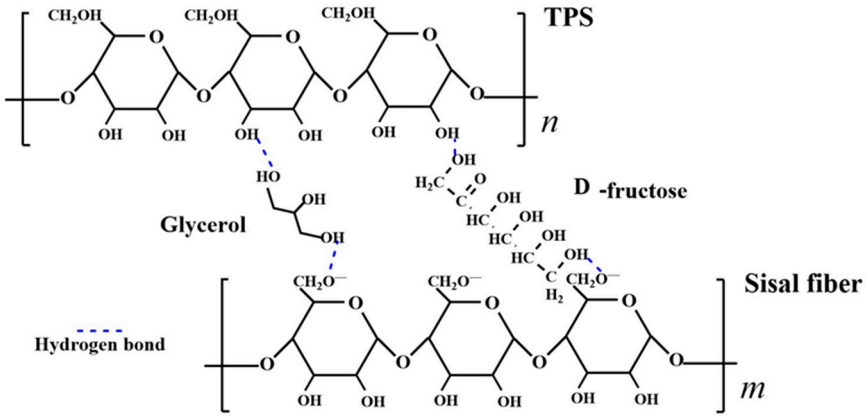


**Figure 10.** A molecular model of hydrogen bond interactions between TPS, plasticizers, and sisal fibers.

*3.4. Parameter optimization of the starch composites*

As an RSM, Box-Behnken design (BBD) is known for its high efficiency, processing speed, and simplicity, and is widely utilized in industrial research. Table 3 presents the results obtained from actual test based on the BBD. The results are used to fit a mathematical model to obtain a response surface, which is then utilized to determine the optimal process parameters.

**Table 3.** Experimental design and results of response surface.

| Experiment number | Forming temperature (°C) | Forming time (min) | AC content (g) | Tensile strength (MPa) | Rebound rate (%) |
|---|---|---|---|---|---|
| **1** | 215 | 6.00 | 1.00 | 1.90 | 64.4 |
| **2** | 195 | 6.00 | 1.00 | 4.02 | 92.5 |
| **3** | 195 | 5.00 | 0.50 | 3.76 | 88.5 |
| **4** | 195 | 4.00 | 1.00 | 3.33 | 87.2 |
| **5** | 205 | 6.00 | 0.50 | 3.4 | 92.4 |
| **6** | 215 | 4.00 | 1.00 | 3.11 | 89.7 |
| **7** | 205 | 5.00 | 1.00 | 3.76 | 94.0 |
| **8** | 195 | 5.00 | 1.50 | 2.88 | 91.6 |
| **9** | 205 | 6.00 | 1.50 | 3.06 | 73.3 |
| **10** | 205 | 5.00 | 1.00 | 4.18 | 95.7 |
| **11** | 205 | 5.00 | 1.00 | 4.10 | 94.5 |
| **12** | 205 | 5.00 | 1.00 | 3.84 | 93.7 |
| **13** | 205 | 4.00 | 1.50 | 1.93 | 84.8 |
| **14** | 205 | 5.00 | 1.00 | 4.23 | 89.4 |
| **15** | 215 | 5.00 | 1.50 | 2.49 | 64.2 |
| **16** | 215 | 5.00 | 0.50 | 2.79 | 73.3 |
| **17** | 205 | 4.00 | 0.50 | 3.31 | 92.1 |

Preprints (www.preprints.org) | NOT PEER-REVIEWED | Posted: 1 August 2023 doi:10.20944/preprints202308.0045.v1



The quadratic polynomial regression model (code) of the forming temperature (A), forming time (*B*), AC content (*C*), tensile strength ($Y_1$), and rebound rate ($Y_2$) is established by second-order polynomial fitting of experimental data. $Y_1$ and $Y_2$ can be expressed as:

$$Y_1=4.02-0.46A+0.088B-0.36C-0.48AB+0.15AC+0.26BC-0.44A^2-0.49B^2-0.60C^2 \quad (6)$$

$$Y_2=0.93-0.085A-0.039B-0.041C-0.077AB-0.031AC-0.029BC-0.081A^2-0.019B^2-0.059C^2 \quad (7)$$

ANOVA was employed to assess the adequacy and significance of the second-order polynomial regression model. The results of variances for tensile strength and rebound rate are presented in Tables 4 and 5, respectively. In these tables, the P-value and LOF are utilized to evaluate the validity of the regression model.

**Table 4.** Variance analysis of second-order polynomial model for tensile strength of samples.

| Coefficient source | Sum of squares | Degree of freedom | variance | p-value |
|---|---|---|---|---|
| model | 7.84 | 9 | 0.87 | 0.0049 |
| A- Forming temperature | 1.71 | 1 | 1.71 | 0.0045 |
| B- Forming time | 0.061 | 1 | 0.061 | 0.4629 |
| C-AC content | 1.05 | 1 | 1.05 | 0.0147 |
| AB | 0.90 | 1 | 0.90 | 0.0205 |
| AC | 0.084 | 1 | 0.084 | 0.3931 |
| BC | 0.27 | 1 | 0.27 | 0.1468 |
| $A^2$ | 0.81 | 1 | 0.81 | 0.0257 |
| $B^2$ | 1.03 | 1 | 1.03 | 0.0155 |
| $C^2$ | 1.53 | 1 | 1.53 | 0.0060 |
| Residual error | 0.71 | 7 | 0.10 | |
| LOF | 0.53 | 3 | 0.18 | 0.1050 |
| Error term | 0.18 | 4 | 0.044 | |
| Total variation | 8.55 | 16 | | |

**Table 5.** Variance analysis of second-order polynomial model for rebound rate of samples.

| Coefficient source | Sum of squares | Degree of freedom | variance | p-value |
|---|---|---|---|---|
| model | 0.16 | 9 | 0.018 | 0.0027 |
| A- Forming temperature | 0.058 | 1 | 0.058 | 0.0007 |
| B- Forming time | 0.012 | 1 | 0.012 | 0.0327 |
| C-AC content | 0.013 | 1 | 0.013 | 0.0282 |
| AB | 0.024 | 1 | 0.024 | 0.0078 |
| AC | 0.0037 | 1 | 0.0037 | 0.1854 |
| BC | 0.0035 | 1 | 0.0035 | 0.1984 |
| $A^2$ | 0.028 | 1 | 0.028 | 0.0051 |
| $B^2$ | 0.0015 | 1 | 0.0015 | 0.3839 |
| $C^2$ | 0.015 | 1 | 0.015 | 0.0220 |
| Residual error | 0.012 | 7 | 0.0017 | |
| LOF | 0.0098 | 3 | 0.0033 | 0.0632 |
| Error term | 0.0022 | 4 | 0.0057 | |
| Total variation | 0.17 | 16 | | |

The P-value of the model serves to determine the influence degree of the parameters on the response. A lower P-value indicates a more significant influence of the parameter on the model,

Preprints (www.preprints.org) | NOT PEER-REVIEWED | Posted: 1 August 2023 doi:10.20944/preprints202308.0045.v1



typically being less than 0.01 [42]. In this investigation, the P-values of the regression model are 0.0049 and 0.0027, respectively, indicating high significance of the model.

LOF compares the disparity between the fitted surface and the actual value with the pure error to assess the capability of the model in representing the actual response surface. Ideally, the LOF should exceed 0.05 [43]. In this investigation, the P-values of the LOF in the regression model are 0.105 and 0.0632, respectively, indicating their lack of significance. Consequently, the model can adequately fit the experimental results.

Adept Precision (AP) represents the ratio of the difference between the maximum and the minimum and predicted values to the average standard deviation of all predicted values. It serves as a measure of the signal-to-noise ratio, and an AP value higher than 4 is considered desirable [44]. In this investigation, the AP values are 7.773 and 10, respectively, indicating an adequate signal level.

Furthermore, the normality of the residuals is assessed through a normal probability graph of the residuals. When the number of models is adequate, the overall shape of the residual graph should resemble a straight line if the residuals follow a normal distribution [45]. Figure 11(a) and (b) display the normal probability plots of the residuals for tensile strength and rebound rate, respectively. The graph depicting the relationship between residuals and the running order can be utilized to identify any correlation between residuals. If a correlation exists among residuals, the assumption of independence will be violated [46]. Figures 11(c) and 11(d) present the effects of run number on residuals of tensile strength and rebound rate, respectively. The random distribution of points indicates that the independence assumption holds for the residuals in this model.

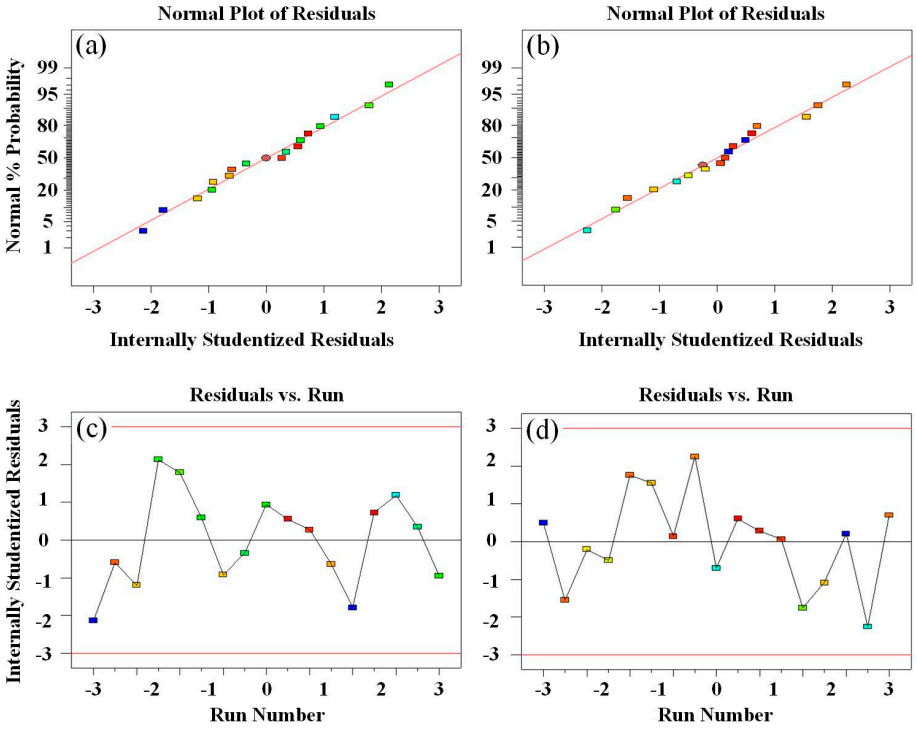


**Figure 11.** Tensile strength and rebound rate of (a, b) residual normal probability graph, (c, d) diagram of the relationship between residuals and running sequence.

Figure 12 depicts the three-dimensional surface and contour plots of tensile strength and rebound rate. In Figures 12(a, a') and 12(d, d'), the AC content is kept constant at 1 gram to investigate the effects of forming temperature and forming time on the mechanical properties of the samples. The results reveal that as the forming temperature and forming time increase, the tensile strength and rebound rate of the sample initially increase and then decrease. This behavior can be attributed to the fact that elevated forming temperature enhances slurry fluidity, facilitates the decomposition of additives, and promotes moisture volatilization within the material, thereby improving the forming

Preprints (www.preprints.org) | NOT PEER-REVIEWED | Posted: 1 August 2023 doi:10.20944/preprints202308.0045.v1



efficiency. However, when the forming temperature becomes excessively high, the tensile strength of the sample remains low, and the rebound rate exhibits a declining trend with increasing forming time. This can be attributed to the detrimental effects of high temperature on the quality of starch and sisal fiber, as well as the generation of uncontrollable gas. Prolonged exposure to high temperatures disrupts the internal structure of the material and adversely affects product quality. Similarly, if the forming time is too short, the slurry fails to mature adequately, resulting in incomplete material formation. Conversely, an excessively long forming time leads to starch and fiber charring, which negatively impacts the mechanical properties of the samples.

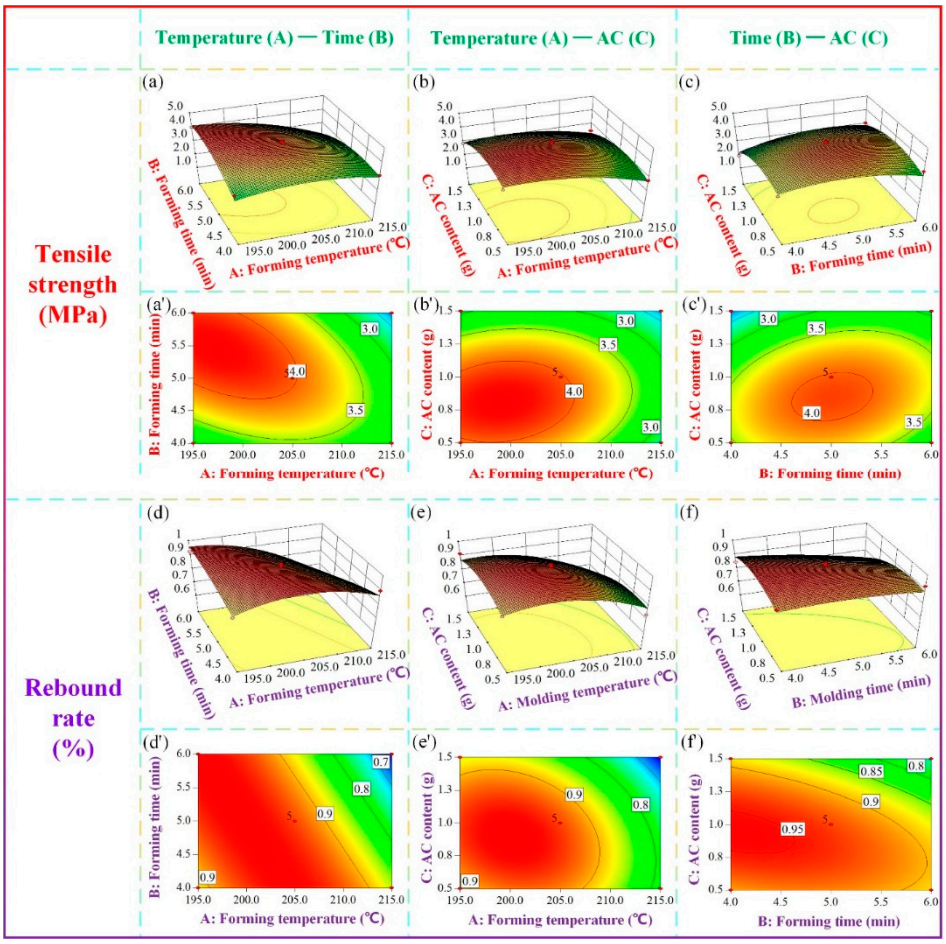


**Figure 12.** Response surface diagrams of (a-c) three-dimensional surface of tensile strength and (a'-c') contour line of tensile strength, (d-f) three-dimensional surface of the rebound rate and (d'-f') contours of the rebound rate.

In Figures 12(b, b') and 12(e, e'), the impacts of forming temperature and AC content on the mechanical properties of the sample are examined with a fixed forming time of 5 minutes. The results indicate that both the tensile strength and rebound rate of the sample decrease as the forming temperature increases, with the minimum values obtained at the highest temperature. Regarding the influence of AC content, the tensile strength and rebound rate initially increase and then decrease with increasing AC content. AC, as the primary power source for the formation of the internal structure of composite materials, significantly affects product quality. Within a reasonable range, increasing the AC content allows for the attainment of a uniform and dense cell structure, which is favorable for foam formation. However, an excessive or insufficient AC content hinders cell formation. When AC undergoes heat-induced decomposition, the resulting gas gradually dissolves in the melt/gas system. If the solubility of the system is exceeded, foaming occurs. During the initial stage of foaming, bubbles of different sizes are generated within the material, with smaller bubbles exerting higher internal pressure. Subsequently, the bubbles enter the growth stage, where they

Preprints (www.preprints.org) | NOT PEER-REVIEWED | Posted: 1 August 2023 doi:10.20944/preprints202308.0045.v1



gather and merge upon contact, gradually forming stable voids. Insufficient AC content impedes foaming and hampers the formation and aggregation of bubbles. Conversely, excessive AC content leads to an excessive amount of gas, making bubble control challenging and increasing the likelihood of bubble rupture, thereby compromising the internal structure and adversely affecting the mechanical properties.

In Figures 12(c, c') and 12(f, f'), the impacts of forming time and AC content on the mechanical properties of the sample are examined at a fixed forming temperature of 205 °C. The results indicate that as the forming time and AC content increase, the tensile strength and rebound rate of the sample initially increase and then decrease, consistent with the findings of the T-t and T-AC experiments.

The optimization process is conducted using the Design Expert software. The optimal process parameters are as follows: the forming temperature (A) is 198.13 °C, the forming time (B) is 5.39 min, and the AC content (C) is 0.84 g. Based on the fitted second-order polynomial mathematical model, the predicted tensile strength is 4.28 MPa, and the rebound rate is 96%. Considering equipment limitations during actual processing, the specific process parameters selected for material preparation are as follows: forming temperature (A) is 198 °C, forming time (B) is 5.4 min, and AC content (C) is 0.84 g. The mechanical properties are then tested. The test results show that the actual process parameters result in a tensile strength of 4.22 MPa and a rebound rate of 95.7%, which are similar to the predicted values generated by the software and mathematical model. This demonstrates the reliability of the RSM for optimizing the forming process of starch-based packaging materials. The process parameters of group 3 in Table 3 are similar to those after optimization, so they are used as the control group without parameter optimization. In comparison with the non-optimized values, the tensile strength of the composite prepared with the optimized process parameters increases by 12.2%, and the rebound rate increase by 8.1%. Additionally, using the optimized process parameters, a starch-based biomass cell phone inner packaging box is prepared, as shown in Figure 13.

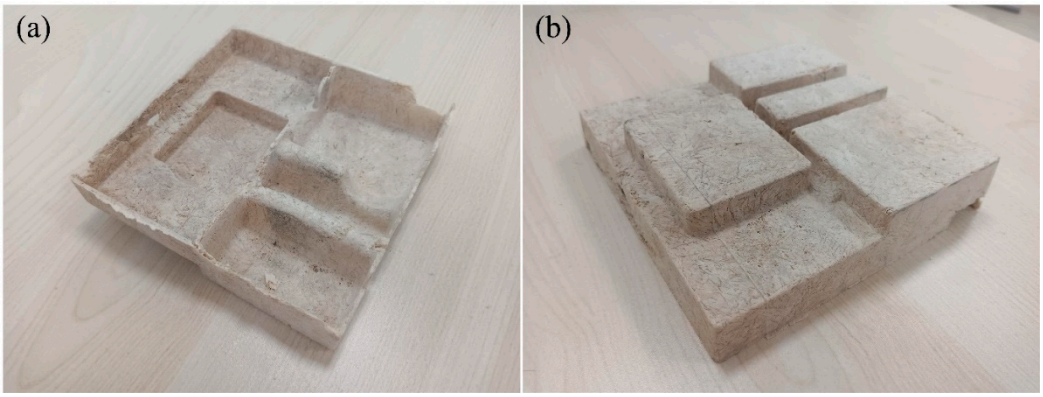


**Figure 13.** A cell phone packaging box made by starch-based biomass composite: (a) top view, and (b) bottom view.

## 4. Conclusions

In this study, processable TPS is prepared by adding plasticizers. It is found that under the influence of plasticizers, the hydrogen bonds of starch are broken, the crystalline peaks decrease, and the granules morphology is disrupted. The use of composite plasticizers resulted in better effects. Subsequently, the preparation of starch-based packaging materials is carried out in a thermal cavity forming machine, and the optimization of the forming process parameters, including forming temperature, forming time, and AC content, is studied using RSM. It is observed that both the tensile strength and rebound rate exhibit an increasing trend followed by a decreasing trend with the increase of the parameters. The optimal mechanical properties are achieved at the process parameters of 198 °C forming temperature, 5.4 minutes forming time, and 0.84 g AC content. Compared to the non-optimized mechanical properties in the experimental design stage, the tensile strength increases by 12.2%, and the rebound rate increases by 8.1%.

**Author Contributions: Conceptualization**, Yue Wu, Anfu Guo, Peng Qu and Shaoqing Wang; **Data curation**, Yue Wu, Xiaodong Tao and Xianliang Sheng; **Investigation**, Xiaodong Tao and Yingbin Hu; **Methodology**, Peng Qu, Shaoqing Wang and Jianfeng Li; **Project administration**, Yue Wu; **Software**, Xianliang Sheng; **Supervision**, Anfu Guo and Yingbin Hu; **Validation**, Yingbin Hu; **Visualization**, Fangyi Li; **Writing – review & editing**, Yue Wu and Rongji Tang.

**Declaration of Competing Interest:** The authors declare that they have no known competing financial interests or personal relationships that could have appeared to influence the work reported in this paper.

**Data Availability:** Data will be made available on request.

**Acknowledgments:** This work is supported by National Natural Science Foundation of China (52075280), Natural Science Foundation of Shandong Province (ZR2023ME154), the Training Program of Innovation and Entrepreneurship for Undergraduates (CXCY2022276), and the start-up funds from the College of Engineering and Computing at Miami University, USA. We also thank Ms. Li Yingchun from Shiyanjia Lab (www.shiyanjia.com) for the EBSD test.

## References

1. Adeniran AA, Shakantu W. The Health and Environmental Impact of Plastic Waste Disposal in South African Townships: A Review. International Journal of Environmental Research and Public Health. 2022;19:779. https://doi.org/10.3390/ijerph19020779.
2. Gaston SA, Tulve NS. Urinary phthalate metabolites and metabolic syndrome in U.S. adolescents: Cross-sectional results from the National Health and Nutrition Examination Survey (2003–2014) data. International Journal of Hygiene and Environmental Health. 2019;222:195-204. https://doi.org/10.1016/j.ijheh.2018.09.005.
3. Hahladakis JN, Velis CA, Weber R, Iacovidou E, Purnell P. An overview of chemical additives present in plastics: Migration, release, fate and environmental impact during their use, disposal and recycling. Journal of Hazardous Materials. 2018;344:179-99. https://doi.org/10.1016/j.jhazmat.2017.10.014.
4. Xu R, Chen F, Ding C. [Opportunities, challenges and suggestions for the development of plastic degradation and recycling under the context of circular bioeconomy]. Sheng wu gong cheng xue bao = Chinese journal of biotechnology. 2023;39:1867-82. https://doi.org/10.13345/j.cjb.221028.
5. Filho WL, Salvia AL, Bonoli A, Saari UA, Voronova V, Klõga M, et al. An assessment of attitudes towards plastics and bioplastics in Europe. Science of The Total Environment. 2021;755:142732. https://doi.org/10.1016/j.scitotenv.2020.142732.
6. Rajvanshi J, Sogani M, Kumar A, Arora S, Syed Z, Sonu K, et al. Perceiving biobased plastics as an alternative and innovative solution to combat plastic pollution for a circular economy. Science of The Total Environment. 2023;874:162441. https://doi.org/10.1016/j.scitotenv.2023.162441.
7. Cheng M-H, Singh S, Carr Clennon AN, Dien BS, Singh V. Production of Designer Xylose-Acetic Acid Enriched Hydrolysate from Bioenergy Sorghum, Oilcane, and Energycane Bagasses. Bioresource Technology. 2023;380:129104. https://doi.org/10.1016/j.biortech.2023.129104.
8. Liu W, Zhang X, Ren H, Hu X, Yang X, Liu H. Co-production of spirosiloxane and biochar adsorbent from wheat straw by a low-cost and environment-friendly method. Journal of Environmental Management. 2023;338:117851. https://doi.org/10.1016/j.jenvman.2023.117851.
9. Suvarnna K, Shanjitha S, Selvasekarapandian S, Kirubavathy SJ. Investigation of solid bio-membrane based on corn biomass as a proton-conducting bio-electrolyte. Bulletin of Materials Science. 2023;46:112. https://doi.org/10.1007/s12034-023-02946-y.
10. Guo A, Tao X, Kong H, Zhou X, Wang H, Li J, et al. Effects of aluminum hydroxide on mechanical, water resistance, and thermal properties of starch-based fiber-reinforced composites with foam structures. Journal of Materials Research and Technology. 2023;23:1570-83. https://doi.org/10.1016/j.jmrt.2023.01.132.
11. Bangar SP, Purewal SS, Trif M, Maqsood S, Kumar M, Manjunatha V, et al. Functionality and Applicability of Starch-Based Films: An Eco-Friendly Approach. Foods. 2021;10:2181. https://doi.org/10.3390/foods10092181.
12. Do Val Siqueira L, Arias CILF, Maniglia BC, Tadini CC. Starch-based biodegradable plastics: methods of production, challenges and future perspectives. Current Opinion in Food Science. 2021;38:122-30. https://doi.org/10.1016/j.cofs.2020.10.020.

13. Jane J-L, Robyt JF. Structure studies of amylose-V complexes and retro-graded amylose by action of alpha amylases, and a new method for preparing amylodextrins. Carbohydrate Research. 1984;132:105-18. https://doi.org/10.1016/0008-6215(84)85068-5.
14. Biduski B, Silva WMFD, Colussi R, Halal SLDME, Lim L-T, Dias ÁRG, et al. Starch hydrogels: The influence of the amylose content and gelatinization method. International Journal of Biological Macromolecules. 2018;113:443-9. https://doi.org/10.1016/j.ijbiomac.2018.02.144.
15. Zhu F, Liu P. Starch gelatinization, retrogradation, and enzyme susceptibility of retrograded starch: Effect of amylopectin internal molecular structure. Food Chemistry. 2020;316:126036. https://doi.org/10.1016/j.foodchem.2019.126036.
16. Cheng W. Preparation and properties of lignocellulosic fiber/CaCO3/thermoplastic starch composites. Carbohydrate Polymers. 2019;211:204-8. https://doi.org/10.1016/j.carbpol.2019.01.062.
17. Zhang B, Xie F, Zhang T, Chen L, Li X, Truss RW, et al. Different characteristic effects of ageing on starch-based films plasticised by 1-ethyl-3-methylimidazolium acetate and by glycerol. Carbohydrate Polymers. 2016;146:67-79. https://doi.org/10.1016/j.carbpol.2016.03.056.
18. Kahvand F, Fasihi M. Plasticizing and anti-plasticizing effects of polyvinyl alcohol in blend with thermoplastic starch. International Journal of Biological Macromolecules. 2019;140:775-81. https://doi.org/10.1016/j.ijbiomac.2019.08.185.
19. Ávila-Martín L, Beltrán-Osuna ÁA, Perilla JE. Effect of the Addition of Citric Acid and Whey Protein Isolate in Canna indica L. Starch Films Obtained by Solvent Casting. Journal of Polymers and the Environment. 2020;28:871-83. https://doi.org/10.1007/s10924-019-01648-z.
20. Zeng G-S, Lin R-Z, Zheng L-J, Chen L, Meng C. Preparation and performance study of waste paper pulp reinforced cornstarch-based composites. 2012;43:2218-21.
21. De Graaf RA, Karman AP, Janssen LPBM. Material Properties and Glass Transition Temperatures of Different Thermoplastic Starches After Extrusion Processing. Starch - Stärke. 2003;55:80-6. https://doi.org/10.1002/star.200390020.
22. Enrione J, Osorio F, Pedreschi F, Hill S. Prediction of the Glass Transition Temperature on Extruded Waxy Maize and Rice Starches in Presence of Glycerol. Food and Bioprocess Technology. 2010;3:791-6. https://doi.org/10.1007/s11947-010-0345-1.
23. Schmitt H, Guidez A, Prashantha K, Soulestin J, Lacrampe MF, Krawczak P. Studies on the effect of storage time and plasticizers on the structural variations in thermoplastic starch. Carbohydrate Polymers. 2015;115:364-72. https://doi.org/10.1016/j.carbpol.2014.09.004.
24. Zdanowicz M, Staciwa P, Spychaj T. Low Transition Temperature Mixtures (LTTM) Containing Sugars as Potato Starch Plasticizers. Starch - Stärke. 2019;71:1900004. https://doi.org/10.1002/star.201900004.
25. Saberi B, Chockchaisawasdee S, Golding JB, Scarlett CJ, Stathopoulos CE. Physical and mechanical properties of a new edible film made of pea starch and guar gum as affected by glycols, sugars and polyols. International Journal of Biological Macromolecules. 2017;104:345-59. https://doi.org/10.1016/j.ijbiomac.2017.06.051.
26. Müller P, Renner K, Móczó J, Fekete E, Pukánszky B. Thermoplastic starch/wood composites: Interfacial interactions and functional properties. Carbohydrate Polymers. 2014;102:821-9. https://doi.org/10.1016/j.carbpol.2013.10.083.
27. Mohammed AABA, Hasan Z, Omran AAB, Kumar VV, Elfaghi AM, Ilyas RA, et al. Corn: Its Structure, Polymer, Fiber, Composite, Properties, and Applications. Polymers. 2022;14:4396. https://doi.org/10.3390/polym14204396.
28. Jenkins PJ, Donald AM. The influence of amylose on starch granule structure. International Journal of Biological Macromolecules. 1995;17:315-21. https://doi.org/10.1016/0141-8130(96)81838-1.
29. Zhang C-W, Li F-Y, Li J-F, Xie Q, Xu J, Guo A-F, et al. Effect of Crystal Structure and Hydrogen Bond of Thermoplastic Oxidized Starch on Manufacturing of Starch-Based Biomass Composite. International Journal of Precision Engineering and Manufacturing-Green Technology. 2018;5:435-40. https://doi.org/10.1007/s40684-018-0046-1.
30. Chen S, Li F-Y, Li J-F, Sun X, Cui J-F, Zhang C-W, et al. Effects of single-modification/cross-modification of starch on the mechanical properties of new biodegradable composites. RSC advances. 2018;8:12400-8. https://doi.org/10.1039/c8ra01592a.

31. Xu Q, Kennedy JF, Liu L. An ionic liquid as reaction media in the ring opening graft polymerization of ε-caprolactone onto starch granules. Carbohydrate Polymers. 2008;72:113-21. https://doi.org/10.1016/j.carbpol.2007.07.031.
32. Zha X, Sadi MS, Yang Y, Luo T, Huang N. Introduction of poly(acrylic acid) branch onto acetate starch for polyester warp sizing. The Journal of The Textile Institute. 2021;112:273-85. https://doi.org/10.1080/00405000.2020.1786260.
33. Pérez-Chávez R, Sánchez-Aguilar J, Calderas F, Maddalena L, Carosio F, Sanchez-Olivares G. A statistical approach to the development of flame retardant and mechanically strong natural fibers biocomposites. Polymer Degradation and Stability. 2022;201:109991. https://doi.org/10.1016/j.polymdegradstab.2022.109991.
34. Singh S, Chakraborty JP, Mondal MK. Pyrolysis of torrefied biomass: Optimization of process parameters using response surface methodology, characterization, and comparison of properties of pyrolysis oil from raw biomass. Journal of Cleaner Production. 2020;272:122517. https://doi.org/10.1016/j.jclepro.2020.122517.
35. Xu Y-Z, Soloway RD, Lin X-F, Zhi X, Weng S-F, Wu Q-G, et al. Fourier transform infrared (FT-IR) mid-IR spectroscopy separates normal and malignant tissue from the colon and stomach. Gastroenterology. 2000;118:A1417. https://doi.org/10.1016/S0016-5085(00)81559-0.
36. Ishkhanyan AM, Krainov VP. Van der Waals Attraction of Hydrogen Atoms. Journal of Experimental and Theoretical Physics. 2021;132:892-6. https://doi.org/10.1134/S1063776121060042.
37. Khatun A, Waters DLE, Liu L. A Review of Rice Starch Digestibility: Effect of Composition and Heat-Moisture Processing. Starch - Stärke. 2019;71:1900090. https://doi.org/10.1002/star.201900090.
38. Shahbazi M, Majzoobi M, Farahnaky A. Impact of shear force on functional properties of native starch and resulting gel and film. Journal of Food Engineering. 2018;223:10-21. https://doi.org/10.1016/j.jfoodeng.2017.11.033.
39. Onyishi HO, Oluah CK. Effect of stretch ratio on the induced crystallinity and mechanical properties of biaxially stretched PET. Phase Transitions. 2020;93:924-34. https://doi.org/10.1080/01411594.2020.1813291.
40. He X, Wu S, Fu D, Ni J. Preparation of sodium carboxymethyl cellulose from paper sludge. Journal of Chemical Technology & Biotechnology. 2009;84:427-34. https://doi.org/10.1002/jctb.2057.
41. Agrawal R, Saxena NS, Sharma KB, Thomas S, Sreekala MS. Activation energy and crystallization kinetics of untreated and treated oil palm fibre reinforced phenol formaldehyde composites. Materials Science and Engineering: A. 2000;277:77-82. https://doi.org/10.1016/S0921-5093(99)00556-0.
42. Idris A, Kormin F, Noordin M. Application of response surface methodology in describing the performance of thin film composite membrane. Separation and Purification Technology. 2006;49:271-80. https://doi.org/10.1016/j.seppur.2005.10.010.
43. Atapour M, Kariminia H-R, Moslehabadi PM. Optimization of biodiesel production by alkali-catalyzed transesterification of used frying oil. Process Safety and Environmental Protection. 2014;92:179-85. https://doi.org/10.1016/j.psep.2012.12.005.
44. Azizi Namaghi H, Mousavi SM. Factorial experimental design for treatment of an industrial wastewater using micellar-enhanced ultrafiltration. Desalination and Water Treatment. 2016;57:5416-24. https://doi.org/10.1080/19443994.2015.1007086.
45. Xiarchos I, Jaworska A, Zakrzewska-Trznadel G. Response surface methodology for the modelling of copper removal from aqueous solutions using micellar-enhanced ultrafiltration. Journal of Membrane Science. 2008;321:222-31. https://doi.org/10.1016/j.memsci.2008.04.065.
46. Lesch SM. Sensor-directed response surface sampling designs for characterizing spatial variation in soil properties. Computers and Electronics in Agriculture. 2005;46:153-79. https://doi.org/10.1016/j.compag.2004.11.004.